Progress In Electromagnetics Research M, Vol. 140, 55–65, 2026
PIER M

(Received 22 July 2026, Accepted 8 September 2026, Scheduled 19 September 2026)

Machine Learning-Based Reflection Coefficient Response Prediction of AMC-PEC Metasurface Antenna Using SVR

Deval Kumar[1,2,*], Somsing Rathod[1], and Amit Kumar Singh[2]

[1]*Electronics & Radar Development Establishment (LRDE), Bangalore 560093, India*
[2]*Department of Electronics Engineering, IIT (BHU), Varanasi 221005, India*

ABSTRACT: Full-wave electromagnetic simulation is computationally intensive during parametric antenna design and optimization. This study proposes a Support Vector Regression (SVR) based framework to predict the reflection coefficient of an Artificial Magnetic Conductor-Perfect Electric Conductor (AMC-PEC) metasurface antenna array in the X-band. The antenna comprises circular AMC cells and rectangular/grid PEC radiating elements arranged in a spatially optimized architecture. A dataset of 500 samples was generated using openEMS full-wave simulations, with antenna geometrical parameters as inputs and S_{11} as the target response. An SVR model with a radial basis function kernel was trained and validated against simulations and measurements of a fabricated multilayer prototype. The predicted, simulated, and measured resonances occurred at approximately 9.8, 9.9, and 10.0 GHz, respectively, while measurements confirmed broadband impedance matching from 9.04 to 11.0 GHz. The SVR achieved a Mean Absolute Error (MAE) of 0.20 dB, Root Mean Square Error (RMSE) of 0.26 dB, and coefficient of determination (R^2) of 0.998, outperforming Artificial Neural Network (ANN) and Gaussian Process Regression (GPR) models trained on the same dataset. Predictions were generated in under one second, providing a speedup of approximately three orders of magnitude over full-wave simulation. The results demonstrate accurate and computationally efficient prediction for antenna design and optimization.

1. INTRODUCTION

Metasurface antennas have attracted considerable research interest due to their ability to control electromagnetic waves through sub-wavelength-engineered structures. Integrating metasurfaces with conventional radiating elements substantially enhances antenna performance, including impedance bandwidth, gain, and radiation efficiency. These properties make metasurface antennas well-suited for applications in wireless communication systems, radar systems, and electromagnetic stealth platforms [1–4, 6].

Despite these advantages, the design and optimization of metasurface antennas typically rely on repeated full-wave electromagnetic simulations, which are time-consuming. Numerical solvers such as HFSS, CST, and openEMS solve Maxwell's equations to compute antenna response. However, parametric sweeps and optimization across multiple geometric variables are computationally intensive, requiring numerous simulations and rendering the design process time-consuming. This is even more important in metasurface antennas, where the resonant frequency, minimum S_{11} value, and -10 dB impedance bandwidth can change slightly owing to geometrical variations [5]. This limitation has been overcome in recent years by using machine learning techniques for antenna modeling and design. Electromagnetic simulation datasets can be used to train machine learning models to learn the nonlinear relationship between antenna geometrical parameters and electromagnetic responses. These models can predict the reflection coefficient response of antenna structures without further full-wave simulations, reducing computational cost and design time in S_{11} optimization [7–10].

Some machine learning regression techniques, including SVR, were benchmarked for direct S_{11} prediction of a patch antenna, further confirming the growing relevance of surrogate-based reflection coefficient modeling within the antenna design community [27]. Most recently, ANN and random forest surrogate models were trained on a smaller dataset of 100 full-wave simulations to predict the $|S_{11}|$, bandwidth, VSWR, gain, and directivity of an elliptical metasurface, defected-ground-structure microstrip antenna [29]. This study reported R^2 values above 0.97 and an approximately 88% reduction in design time relative to conventional parametric sweeps, although the authors noted that their results were simulation-based and had not yet been experimentally validated. Subsequently, [30] extended this surrogate modeling approach to both the forward and inverse designs of a metasurface-loaded microstrip antenna, comparing Gradient Boosting, Random Forest, XGBoost, and K-Nearest Neighbors regressors on a larger dataset of 1,118 samples and validated the design against a fabricated prototype, noting that Random Forest achieved the most balanced accuracy for the inverse task. More broadly, [28] reviewed AI-assisted metasurface antenna design and optimization across forward and inverse design paradigms, spanning frequency-selective surfaces, absorbers, polarization surfaces, multiple-input multiple-output (MIMO), horn, and leaky-wave configurations, underscoring

* Corresponding author: Deval Kumar (devalkumar.rs.ece21@itbhu.ac.in).

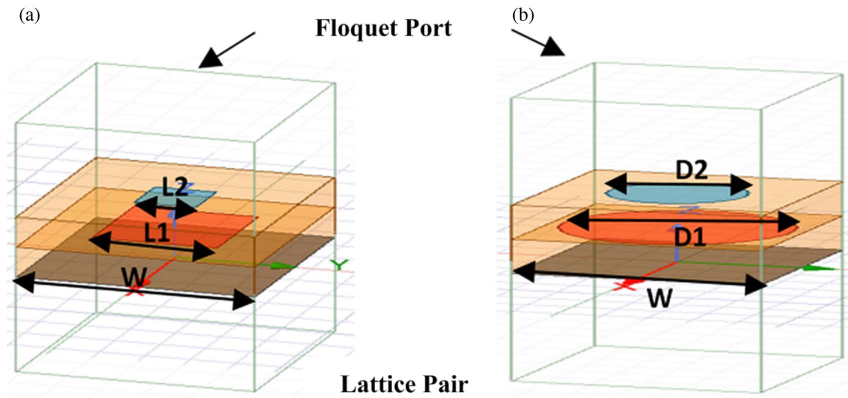

FIGURE 1. (a) PEC unit cell and (b) AMC unit cell.

the breadth and pace of AI adoption in the metasurface antenna design landscape.

Support Vector Regression (SVR) is well-suited for nonlinear regression problems involving moderate-sized datasets. SVR is used to estimate complex nonlinear correlations between the input variables and the model's high-dimensional feature space by employing kernel functions [11, 12]. SVR has been effectively used to solve the problems in antenna parameter prediction and electromagnetic modeling [15]. Open-source electromagnetic simulation software, including openEMS, has also gained popularity for antenna modeling and dataset generation. openEMS is a Finite-Difference Time-Domain (FDTD) electromagnetic solver that enables parsimonious parametric simulations and dataset generation [14]. Machine learning models can be trained to predict antenna performance based on simulation-based datasets produced using openEMS.

This study presents a machine learning-based predictive framework for estimating the S_{11} response of a metasurface antenna. A set of 500 antenna configurations was generated using parametric simulations with the openEMS software by varying the most important geometric parameters. The dataset was used to train an SVR model to predict the reflection coefficient response of the AMC-PEC metasurface antenna array. The S_{11} response of the fabricated antenna was compared with the full-wave simulated response of a reference metasurface antenna design, and the results were also compared with the predicted S_{11} response. The proposed structure demonstrates the feasibility of using machine-learning-based modeling for fast estimating S_{11} and optimizing AMC-PEC metasurface antenna arrays while minimizing full-wave simulation time.

2. ANTENNA DESIGN

An X-band metasurface antenna array was designed employing a spatially optimized AMC-PEC architecture, unlike prior designs that distribute AMC and PEC cells in a uniform alternating checkerboard pattern. The surface response of the antenna aperture is controlled by the AMC-PEC arrangement without affecting its radiation behavior. The antenna geometry was considered primarily to predict the reflection coefficient and validate the antenna impedance bandwidth. The antenna's S_{11} response was determined by the combined arrangement of PEC radiating elements, AMC cells, aperture-coupled slots, and feeding network.

2.1. Unit Cell Design

The metasurface was fabricated using two types of unit cells: a PEC cell and an AMC cell.

Figure 1 shows the geometrical structures of the unit cells. A square metallic patch was used to implement the PEC unit cell, and a circular metallic patch geometry was used to implement the AMC unit cell. A circular AMC geometry was used, which offers a smoother phase variation and better angular stability than conventional square AMC elements. The two unit cells were composed of multilayer dielectric substrates and metallic layers. The dielectric layers were made of Rogers RT/duroid 5880 substrate with ε_r of 2.2 and $\tan\delta$ of 0.0009 at 10 GHz. In the unit cell simulations, periodic boundary conditions incorporating the Floquet port were used to evaluate the reflection properties of the metasurface elements. Unit cell dimensions were optimized, as shown in Table 1. These parameters were obtained by parametric optimization to ensure that the reflection magnitudes of both cells were more or less the same, but at the same time, there was a reflection phase difference of approximately 180° throughout a broad frequency range.

2.2. Reflection Phase Characteristics

Reflection phase responses of PEC and AMC unit cells were analyzed to confirm the phase behavior of the metasurface structure. Fig. 2 shows the simulated results for the reflection phase characteristics at normal and 10° incidence angles.

The phase difference between the two unit cells does not change significantly over the frequency range of 7–13 GHz and is at approximately 180°, with deviations of approximately 30°. To further study the metasurface's angular stability, reflection phases were also considered at an incident angle of 10°. The difference in the phase of the PEC and AMC cells does not change significantly with frequency in the frequency range in question, which implies that the metasurface structure retains the same reflection characteristics when the incidence is oblique. The stable phase behavior suggests that the metasurface structure has a stable electromagnetic response in the

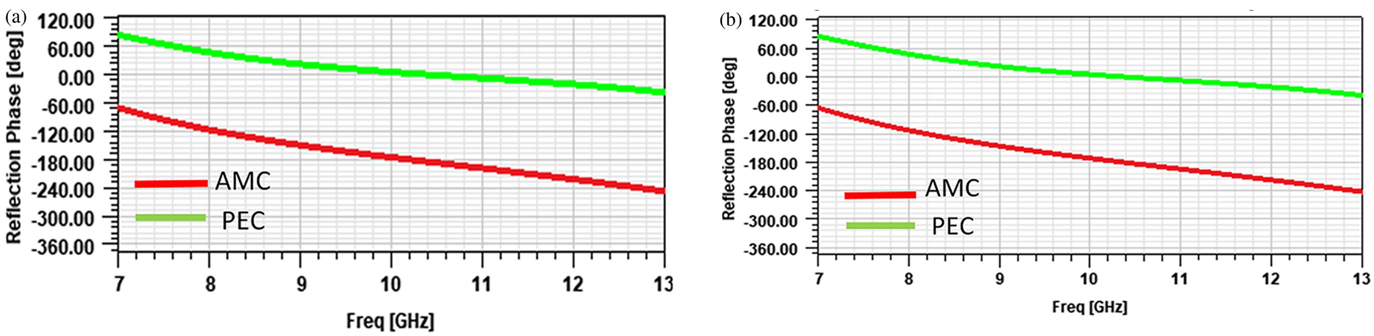

FIGURE 2. (a) Phase difference for 0 incident angle and (b) phase difference for 10 incident angle.

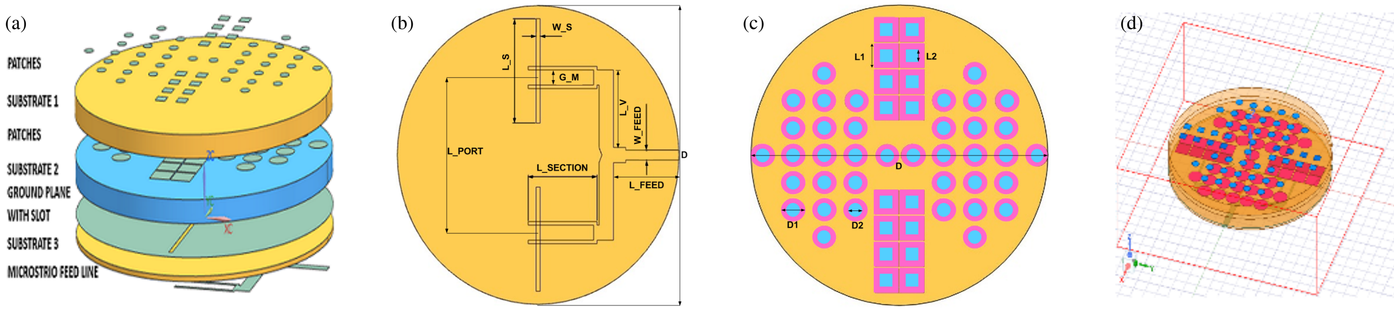

FIGURE 3. AMC-PEC metasurface schematic. (a) Detailed schematic design, (b) T-power divider, (c) schematic design of PEC & AMC cells, and (d) simulation model.

desired X-band. The circular AMC components were mounted on the radiating PEC cells to ensure that the required phase contrast is maintained with a minimal influence on radiation performance.

2.3. Metasurface Antenna Array Configuration

The metasurface antenna array was fabricated by spatially distributing PEC and AMC unit cells after optimization. Fig. 3 shows the general design of the proposed antenna array. The antenna has four metal and three dielectric layers of Rogers RT/duroid 5880, with a thickness of 3.17 mm, integrated into a multilayer structure. The antenna array feeding network was fabricated using a T-junction power divider that provides same amplitude and phase signals to the radiating elements. It uses aperture coupling between the feed network and radiating patches using slots cut into the ground plane. In this arrangement, power is efficiently transferred between the feed network and radiating patches.

The rectangular radiating patches were patterned with grid slots to enhance the operational bandwidth. These grid-slot patches also act as PEC cells and radiating elements of the antenna array. The circular AMC components were mounted on the radiating PEC cells to ensure that the required phase contrast was maintained with a minimal influence on radiation performance.

2.4. Design Parameters

Table 1 lists complete dimensions of the proposed antenna array, as shown in Fig. 3(b) and Fig. 3(c). The parameters were selected to provide stable radiation performance and broadband impedance matching in the X-band frequency range. The optimized dimensions were used as the reference geometry for generating the datasets and predicting S_{11} for openEMS. A small antenna size is ideal for X-band wireless and radar applications, where a low profile and stable impedance response are desired. The antenna array was 68.74 mm in diameter, which corresponds to $4.12\lambda_0^2$ at 10 GHz. This small form can be easily incorporated into airborne radar systems, which require a low profile and minimal electromagnetic scattering.

TABLE 1. Design parameters.

Parameters	Value (mm)
D	68.74
$L1$	5.5
$L2$	2.72
$D1$	6
$D2$	3
W_Feed	2.3
L_s	24
W_s	1
L_section	16.8
L_V	18.2
L_Port	36.7
L_Feed	18.9
G_M	3.4
Substrate Thickness (h)	3.17

2.5. Geometric Parameter Impact Analysis

The relative importance of each geometrical parameter was quantified using permutation feature-importance analysis to predict the S_{11} response using the SVR, as shown in Fig. 4. This method was used because the coefficients of original input variables were not available for the Radial Basis Function (RBF)-SVR model. The values of each variable were permuted, while the other variables were kept constant, and the change in prediction error was noted for each variable. Parameters that caused a greater decrease in predictive accuracy were assigned a higher weight. Permutation importance is the decrease in model prediction accuracy when the values of one input parameter are randomly permuted, and the other parameters are kept fixed. The larger the permutation importance score, the more important the parameter is for SVR prediction, and the closer it is to zero, the less important the parameter is for the prediction within the design space investigated. The analysis revealed that parameters $D1$, $D2$, W_s, and h had a relatively high permutation importance and were the most important parameters influencing the S_{11} response. D1 and D2 influenced effective resonant dimensions of the patch structure; W_s influenced the ground-plane current path and electromagnetic coupling; and h influenced the effective electrical thickness and field distribution. The permutation importance of the other geometrical parameter, W_Feed, was lower over the investigated ranges than other parameters. The results confirm the choice of the AMC unit-cell patch size, the PEC patch size, the slot width, and the substrate thickness as main geometrical parameters for the parametric study.

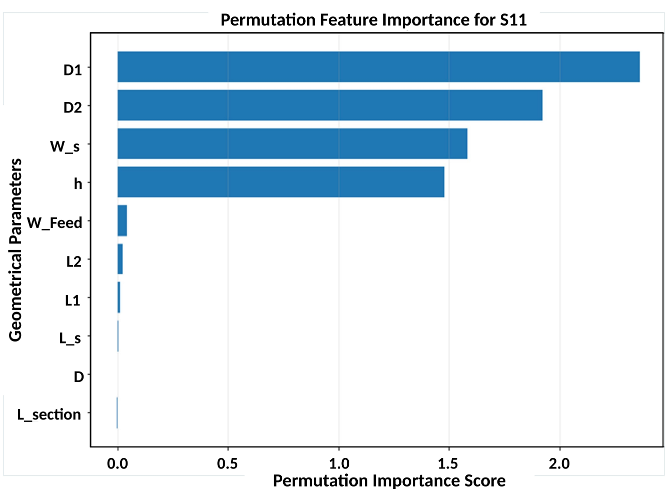

FIGURE 4. Permutation feature importance for the geometrical parameters.

3. DATASET GENERATION USING OPENEMS

The electromagnetic characteristics of the metasurface antenna, as explained in Section 2, depend on several geometrical parameters associated with PEC radiating elements, AMC unit cells, slot geometry, and feeding network. Although the optimized antenna design achieved the desired radiation and scattering properties, the interaction between the antenna geometry and electromagnetic response was strongly nonlinear. Thus, full-wave simulation-based data were developed to establish a predictive relationship between the variables of antenna design and electromagnetic performance.

The dataset was developed using the openEMS electromagnetic solver based on the FDTD method [14]. The metasurface antenna model outlined in Section 2 was used as the base structure, and automated parametric simulations were performed by varying the antenna's significant geometrical parameters. The primary parameters varied included the AMC unit cell patch size (range: 4–8 mm), the PEC patch size (range: 3–7 mm), the slot width in the ground plane (range: 0.6–1.2 mm), and the substrate thickness (range: 2.5–4.0 mm). 500 unique parameter combinations were generated using Latin Hypercube Sampling (LHS) strategy to ensure uniform coverage of the design space. Each openEMS simulation required approximately 8–12 minutes on a standard quad-core workstation, resulting in a total dataset generation time of approximately 70–100 hours. Once trained, the proposed SVR surrogate model produces predictions in less than one second per query, representing a speedup of up to three orders of magnitude relative to the full-wave simulation. The antenna was excited through a lumped excitation port in contact with the feeding network, and Perfect Matching Layer (PML) absorbing boundaries were applied at the cell walls of the simulation domain. The time-domain electromagnetic response was converted to the frequency domain via Fourier analysis to obtain reflection coefficient ($|S_{11}|$) characteristics across the X-band. Fig. 5 illustrates the complete data generation workflow, beginning with the definition of the geometrical parameters and the storage of the annotated electromagnetic response dataset for surrogate model training.

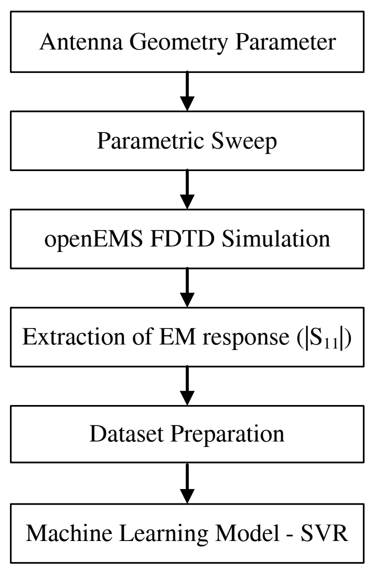

FIGURE 5. Process workflow of dataset generation based on openEMS parametric simulation.

A set of geometrical parameters was varied in the parametric sweep, as listed in Table 1, including dimensions of the AMC unit cell, PEC patch, slot geometry, and feeding network. The parameter ranges were selected to span a sufficiently large design space while ensuring that all configurations corresponded to physically realizable antenna structures. Each data sample consisted of geometrical input parameters and the corresponding electromagnetic responses extracted from the openEMS simulation. The dataset can be expressed as

$$D = \{(X_i, Y_i)\}_{i=1}^{N} \tag{1}$$

X_i is a set of antenna design parameters; Y_i is the electromagnetic response in the simulation; and $N = 500$ is the total number of samples. The data were divided into feature vectors and target outputs, with geometrical parameters as the input feature and electromagnetic responses as the prediction targets. The data were split into training and testing sets to evaluate the prediction ability of the regression model. The SVR model was then trained to predict the electromagnetic performance of the metasurface antenna directly based on geometrical parameters without any further electromagnetic simulation, as explained in the following section.

4. SUPPORT VECTOR REGRESSION FOR PREDICTION OF ANTENNA RESPONSE

Electromagnetic properties of the metasurface antenna show strong nonlinearity, and the relationship between the geometrical parameters of AMC-PEC unit cells and electromagnetic responses, such as reflection coefficient and scattering characteristics, is complex and cannot be adequately represented by a linear model. To address this, a statistical learning regression model was employed to establish the mapping between the antenna geometrical parameters and the full-wave simulation electromagnetic responses. SVR was selected as the predictive modeling approach. SVR is a generalization of the Support Vector Machine (SVM), which was initially proposed to deal with classification problems but was subsequently generalized by Vapnik [18] into an ε-insensitive regression model of nonlinear regression with high generalization behavior [19]. The capability to predict nonlinear relationships with comparatively small training sets has made SVR an extremely popular choice for engineering prediction problems [18–21]. Recently, machine learning techniques have been applied to antenna engineering to generate surrogate models of electromagnetic simulations, in which the antenna reaction is predicted as a direct function of geometrical values, eliminating the need to execute repeated electromagnetic simulations. It has been previously established that machine learning models based on Gaussian Process Regression and Support Vector Regression can be used to predict antenna parameters, including resonance frequency, gain, and reflection coefficient, with high accuracy and save time in antenna design [16, 17]. Thus, the dataset obtained from the openEMS simulations was applied to the SVR in this study to predict the electromagnetic performance of the metasurface antenna.

Figure 6 shows the SVR model and illustrates the workflow in predicting the antenna response. The openEMS simulation generates a sample that is manipulated to identify the geometrical characteristics involved in training the SVR model. The trained model identifies the support vectors and predicts the antenna responses as reflection coefficients. Prediction accuracy was determined using statistical measures. The purpose of SVR is to find a regression model that can approximate the relationship between input variables and the target value. The regression equation can be expressed as follows:

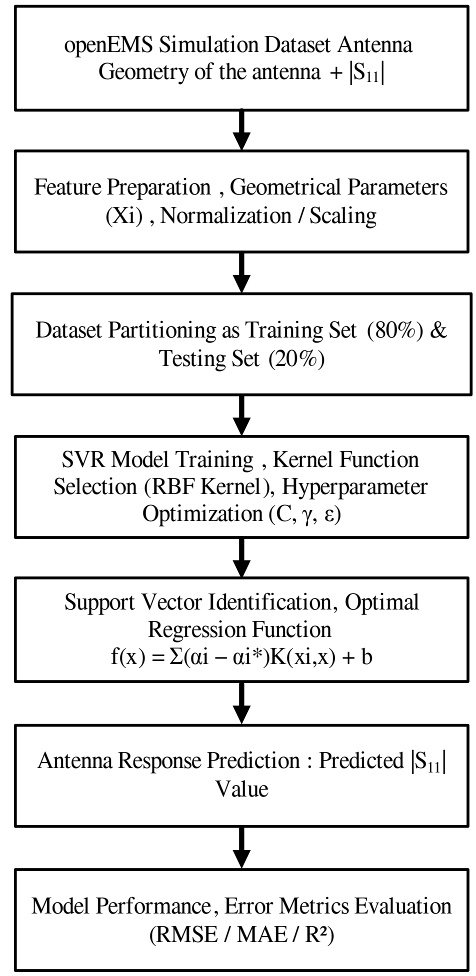

FIGURE 6. Workflow related to the SVR model.

$$f(x) = w^T \emptyset (x) + b \tag{2}$$

w is the weight vector; b is the bias term; and $\phi(x)$ is a nonlinear mapping that changes the input vector into a higher-dimensional feature space. Its objective is to seek a function that has low complexity and adapts within a given tolerance to the training data.

The SVR optimization problem is designed based on the ε-insensitive loss function that takes non-penal errors within a threshold ε. The optimization problem can be formulated as

$$\min_{w,b,\varepsilon_i,\varepsilon_i^*} \frac{1}{2}\|w\|^2 + C\sum_{i=1}^{N}(\varepsilon_i + \varepsilon_i^*) \tag{3}$$

subject to

$$y_i - \left(w^T \emptyset (x_i) + b\right) \leq \varepsilon + \varepsilon_i$$

$$\left(w^T \emptyset (x_i) + b\right) - y_i \leq \varepsilon + \varepsilon_i^*$$

$$\varepsilon_i, \varepsilon_i^* \geq 0$$

where C is the regularization parameter that trades off model complexity and training error, and ξ_i, ξ_i^* are slack variables that permit deviation outside the ε-insensitive region. The Lagrange

TABLE 2. Comparative analysis of SVR predicted, simulated and measured results.

Parameter	Predicted	Simulated	Measured
Resonant frequency	9.8 GHz	9.9 GHz	10.0 GHz
-10 dB impedance bandwidth	8.8–11.7 GHz	8.8–11.6 GHz	9.04–11.0 GHz

multipliers can convert the above optimization problem into a dual problem. The resulting regression equation is as follows:

$$f(x) = \sum_{i=1}^{N} (\alpha_i - \alpha_i^*) K(x_i, x) + b \tag{4}$$

where $K(x_i, x)$ is referred to as the kernel function, and α_i, α_i^* are referred to as Lagrange multipliers. A regression model is represented by a kernel function with nonlinear relationships that are not explicit computations using the high-dimensional mapping $\phi(x)$. The training examples used to build the regression model are only a subset of all training examples; they are called support vectors.

In nonlinear electromagnetic modeling problems, the Radial Basis Function (RBF) kernel is popular because it effectively captures smooth nonlinear variations in nonlinear regression problems [19]. The RBF kernel is defined as:

$$K(x_i, x_j) = \exp(-\gamma \parallel x_i - x_j \parallel^2) \tag{5}$$

where γ defines the diffusion of the kernel function.

The RBF kernel was used because the mapping between geometrical variables and the S_{11} response is nonlinear and not conveniently represented by a prescribed analytical form. The linear kernel assumes a hyperplane relationship, whereas the polynomial kernel requires the order of the polynomial to be known beforehand. The RBF formulation does not impose such restrictions and can thus be used to model the coupled, resonance-dependent response of the metasurface antenna. To test the choice of kernel, the linear, third-order polynomial, and RBF kernels were tested with the same training and test partitions. They are compared in terms of prediction errors in Section 5.

In this study, SVR was used as a surrogate for the full-wave electromagnetic model. The model was trained with responses from the openEMS dataset and then used to estimate S_{11} for the geometrical configurations in the sampled design space. Therefore, no full-wave analysis was required for each model evaluation, thus alleviating the computational load of design exploration.

SVR, ANN, and GPR models were implemented in Python using the Scikit-learn library [13]. The predictive accuracy of the SVR model depends on three key hyperparameters: the regularization parameter C, RBF kernel width γ, and width of the ε-insensitive tube. These hyperparameters were tuned using a grid search combined with five-fold cross-validation on the training subset, over the ranges $C \in \{1, 10, 100, 1000\}$, $\gamma \in \{0.001, 0.01, 0.1, 1\}$, and $\varepsilon \in \{0.001, 0.01, 0.1\}$. The combination yielding the lowest cross-validated RMSE was adopted as the final configuration: $C = 100$, $\gamma = 0.01$, and $\varepsilon = 0.01$. All geometrical input features were normalized to the range [0, 1] before training to prevent parameters with larger numerical ranges (e.g., substrate thickness in mm) from dominating the RBF kernel's distance computation. The target output, S_{11} in dB, was not normalized because dB is already a logarithmic, compressed representation of a power ratio and does not show the same raw-scale disparity that motivates input normalization, and reporting error metrics directly in dB (Table 3) preserves the direct physical interpretability of the reported MAE and RMSE values. The dataset of 500 samples was partitioned into training and testing subsets using an 80/20 split (400 training and 100 testing samples), with the testing subset withheld from the hyperparameter search to provide an unbiased estimate of the generalization performance reported in Section 5.

TABLE 3. Prediction performance measures of machine learning.

Parameters	MAE (dB)	RMSE (dB)	R^2
S_{11}	0.20	0.26	0.998

5. RESULTS AND DISCUSSION

The predictive performance of the trained SVR model was evaluated by comparing the predicted S_{11} response with corresponding full-wave simulated and experimentally measured responses of the proposed AMC-PEC metasurface antenna. A comparison was performed to assess the accuracy of the proposed surrogate model in predicting the reflection coefficient over the X-band operating frequency range and to demonstrate its capability for rapid antenna response estimation with significantly reduced computational effort.

Fig. 7(a) shows the fabricated prototype of the multilayer AMC-PEC metasurface antenna. The structure comprises patterned metasurface layers, a Rohacell spacing layer, and a microstrip radiating section in a compact multilayer structure. Circular AMC elements and rectangular/grid-based PEC radiating elements were fabricated with optimized dimensions, as in the simulation model. Fig. 7(b) shows the experimental setup. The fabricated antenna was supported by low-reflection foam absorbers to minimize unwanted reflections during the measurement. A Vector Network Analyzer (VNA) was used to measure the antenna response. Fabricated antenna parameters were measured, and results were compared with simulated ones to verify the impedance-matching behavior in the X-band. The measured response agrees with the simulated response and validates broadband impedance matching up to 11.0 GHz.

Fig. 8 presents a comparison among the SVR-predicted, full-wave simulated, and experimentally measured S_{11} responses. The SVR model predicts a resonance at approximately 9.8 GHz with a minimum S_{11} of approximately -31 dB, whereas the full-wave simulation predicts a resonance near 9.9 GHz with a minimum S_{11} of approximately -30 dB. The correspond-

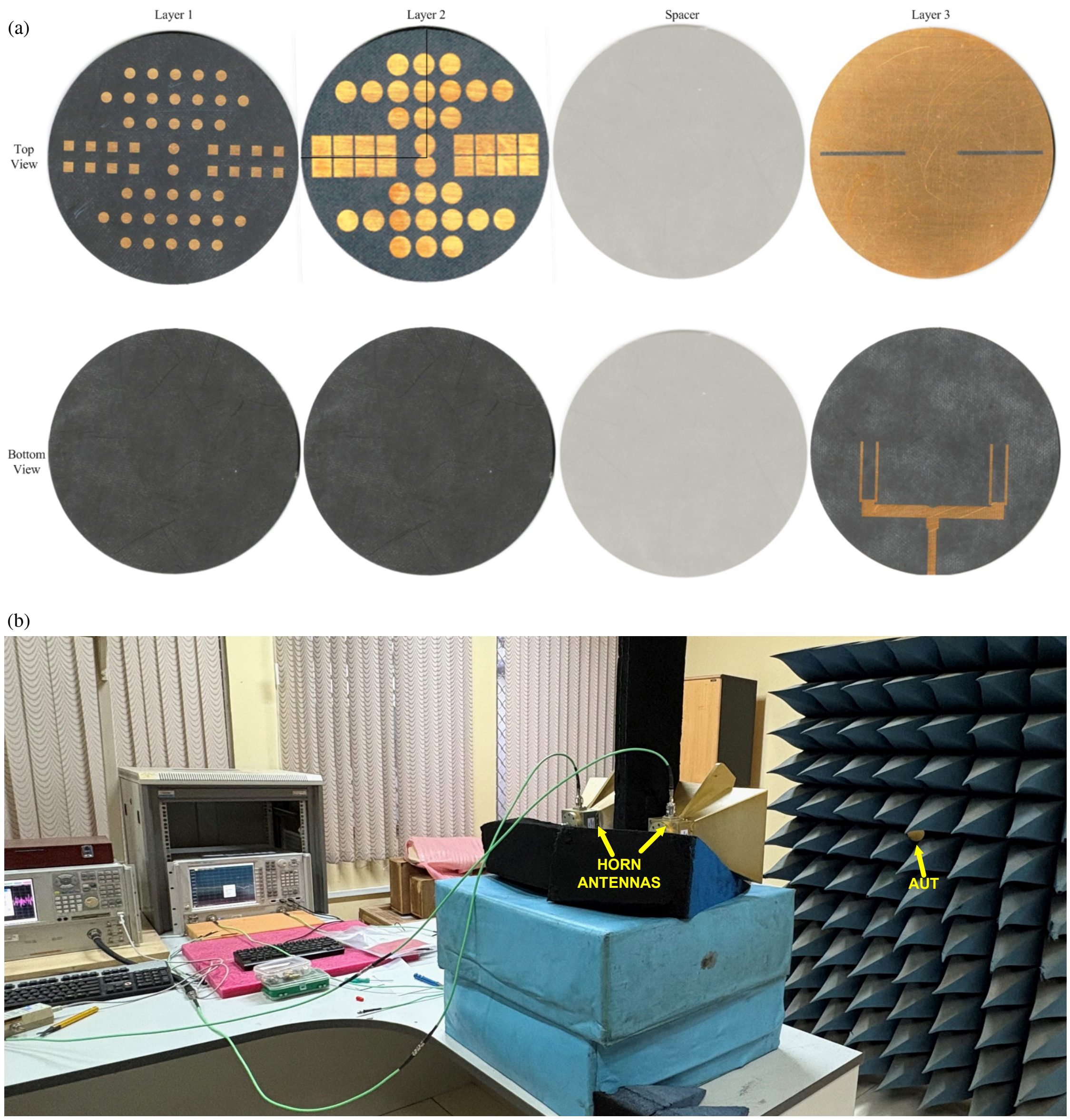

FIGURE 7. (a) Fabricated multilayer metasurface antenna and (b) complete test setup for S_{11} measurement.

ing -10 dB impedance bandwidths were 8.8–11.7 GHz and 8.8–11.6 GHz, respectively, indicating excellent agreement between predicted and simulated responses. The measured antenna exhibited a resonance near 10.0 GHz with a minimum S_{11} of approximately -22 dB and maintained a -10 dB impedance bandwidth over 9.04–11.0 GHz. The observed deviations between the simulated and measured responses were primarily attributed to substrate tolerances, fabrication variations, connector transition effects, and measurement uncertainties. The SVR predicts the response of the idealized simulated geometry represented in the training dataset; therefore, the difference between the SVR prediction and the measured response primarily reflects the same fabrication and measurement-related deviations that cause simulation-to-measurement discrepancy. The close agreement between the SVR and full-wave simulated responses confirms that the observed deviation from measurement is not primarily attributable to the surrogate model. Nevertheless, the measured response confirmed the broadband impedance characteristics of the fabricated antenna and experimentally validated the proposed design.

Table 2 presents a quantitative comparison of the SVR-predicted, full-wave simulated, and measured S_{11} characteristics. The close agreement between the predicted and simulated resonant frequencies, minimum S_{11}, and impedance bandwidths demonstrates the high accuracy of the proposed SVR model. Furthermore, the experimental results verified that the surrogate model accurately predicted the reflection coefficient while substantially reducing the dependence on computationally expensive full-wave electromagnetic simulation.

In addition to the graphical comparison, the predictive accuracy of the regression model was quantitatively evaluated using three standard statistical performance metrics: Root Mean Square Error (RMSE), Mean Absolute Error (MAE), and coefficient of determination (R^2), defined by Eqs. (6)–(8), respec-

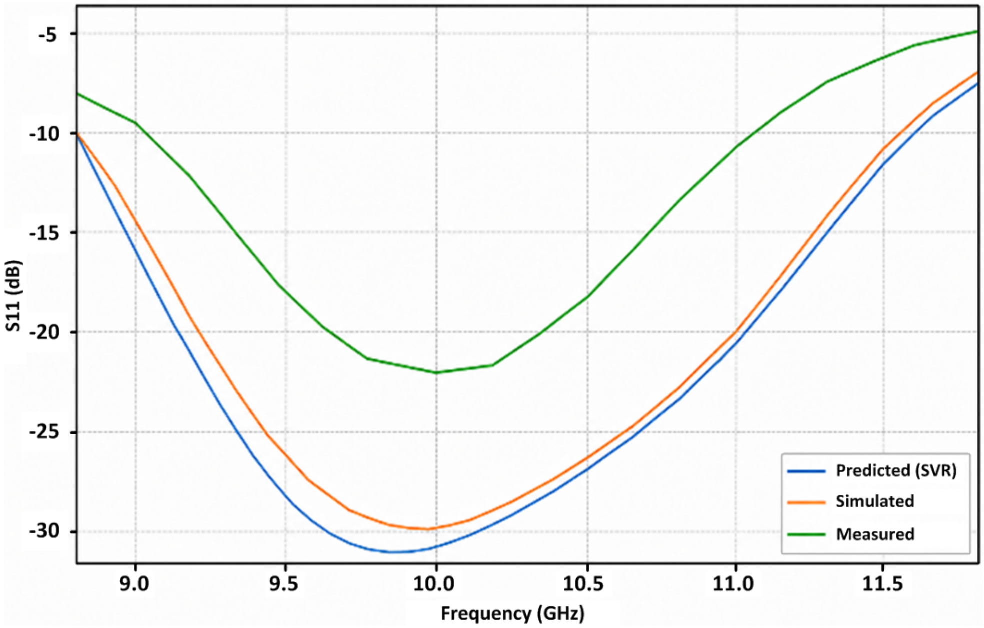

FIGURE 8. Comparison of simulated vs predicted vs measured S_{11}.

tively. These metrics quantify the agreement between the SVR-predicted and full-wave simulated S_{11} responses.

$$\mathrm{RMSE} = \sqrt{\frac{1}{N}\sum_{i=1}^{N}(y_i - \hat{y}_i)^2} \tag{6}$$

$$\mathrm{MAE} = \frac{1}{N}\sum_{i=1}^{N}|y_i - \hat{y}_i| \tag{7}$$

$$R^2 = 1 - \frac{\sum(y_i - \hat{y}_i)^2}{\sum(y_i - \bar{y})^2} \tag{8}$$

Table 3 summarizes performance metrics of the proposed SVR model. An MAE of 0.20 dB, RMSE of 0.26 dB, and R^2 value of 0.998 indicate excellent agreement between the predicted and simulated responses.

The low error values and high coefficient of determination demonstrate that the proposed SVR model effectively captures the nonlinear relationship between antenna geometrical parameters and corresponding reflection coefficient response.

To assess how sensitive the SVR model is to the choice of hyperparameters, the RMSE was calculated using five-fold cross-validation throughout the entire grid search space. Fig. 9 shows RMSE values over the C-γ search space at $\varepsilon = 0.01$. The mean cross-validation RMSE was approximately 0.360 dB for the adopted configuration $C = 100$ and $\gamma = 0.01$. The difference between the error surfaces shows the influence of the regularization parameter and the RBF-kernel parameter on prediction accuracy and provides another indication of the choice of hyperparameters.

Linear, third-order polynomial, and RBF-SVR models were also compared with the same training and testing subsets to further investigate the choice of kernel. Table 4 summarizes the obtained prediction metrics.

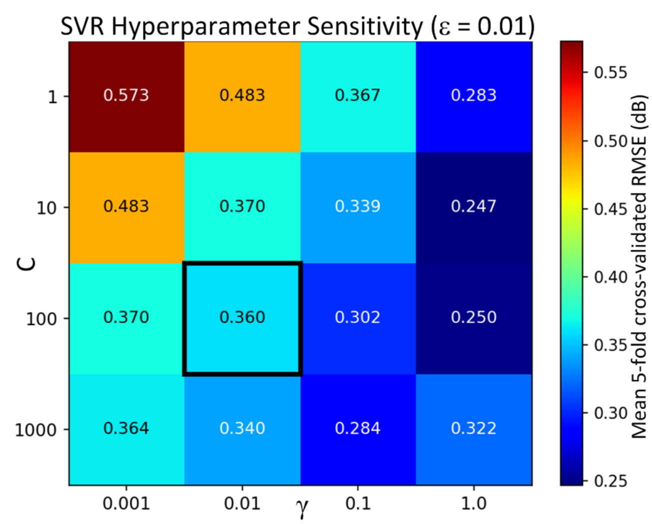

FIGURE 9. RMSE sensitivity of the SVR model to C and γ for $\varepsilon = 0.01$ using five-fold cross-validation.

TABLE 4. Comparison of S_{11} prediction performance for different SVR kernels.

Kernel	MAE (dB)	RMSE (dB)	R^2
Linear	0.32	0.42	0.993
Polynomial	0.31	0.41	0.994
RBF	0.20	0.26	0.998

All three kernels were accurate in predicting the data, with the nonlinear polynomial and RBF kernels having slightly lower RMSE than the linear kernel. The RMSE and R^2 values of polynomial and RBF models were practically the same, and MAE values were only slightly different. The RBF kernel was chosen because it is a nonlinear representation of the geometry-to-S_{11} relationships and does not require the polyno-

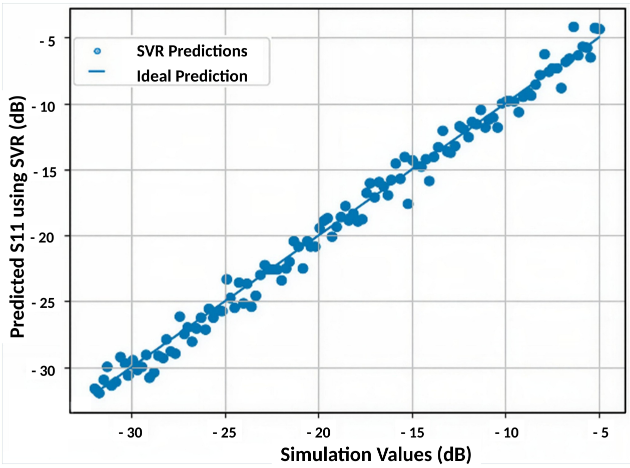

FIGURE 10. Predicted vs Simulated S_{11} values.

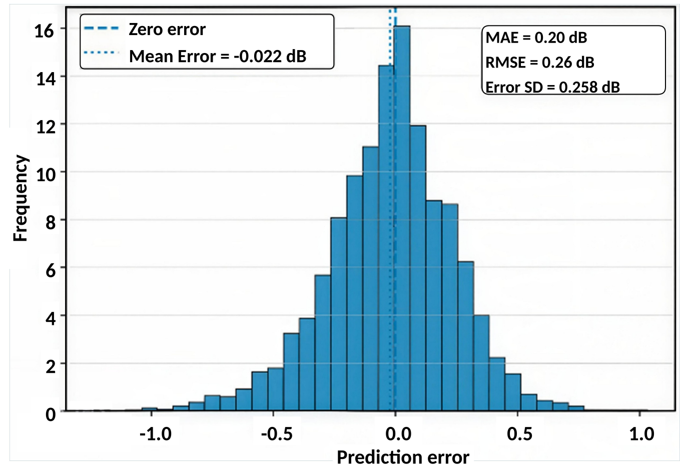

FIGURE 11. Distribution of prediction error (predicted-simulated) for the testing dataset.

TABLE 5. Comparison of SVR with alternative machine learning regression models.

Model	ANN	GPR	SVR (Proposed)
MAE (dB)	0.48	0.23	0.20
RMSE (dB)	0.65	0.34	0.26
R^2	0.985	0.996	0.998
MAE reduction with SVR	**58.3%**	**13.0%**	**Ref.**
RMSE reduction with SVR	**60.0%**	**23.5%**	**Ref.**

mial order to be known a priori. This is a desirable property for the couple, resonance-dependent electromagnetic response that is the subject of the present study.

To further assess the effectiveness of the proposed approach, the prediction performance of the SVR model was benchmarked against two other widely used machine learning regression techniques: an Artificial Neural Network (ANN) and Gaussian Process Regression (GPR) [22]. Both benchmark models were trained and evaluated on the same 500-sample openEMS dataset and the same 80/20 train-test split as the SVR model, using identical geometrical input features and S_{11} response as the target output. Table 5 compares the prediction accuracies of the three regression models. The proposed SVR model achieved the lowest prediction error and the highest coefficient of determination among the three regression techniques. Compared to GPR, the proposed SVR model achieves improvement in MAE and RMSE by 13.0% and 23.5%, respectively. Compared to ANN, these improvements are 58.3% and 60.0%, respectively. Although the GPR model provides competitive performance, its prediction accuracy remains slightly inferior to the proposed SVR model, whereas the ANN model has a comparatively larger prediction error.

The superior performance of the RBF-kernel SVR can be attributed to its ability to effectively model nonlinear relationships using a moderately sized training dataset, making it particularly suitable for the surrogate modeling of metasurface antenna responses.

The computational effort required for model development was also assessed. The hyperparameter search consisted of 48 combinations of C, γ, and ε, which were tested with five-fold cross-validation, resulting in 240 fits of SVR. The total grid search time was approximately 79.17 s on an Intel-based Windows workstation. This is an offline cost that occurs only during model selection and is relatively small compared to the 500-sample full-wave simulation data taking about 70–100 hours to generate.

In addition to its high prediction accuracy, the proposed SVR model generates predictions in less than one second after training, whereas a single full-wave openEMS simulation requires approximately 8–12 minutes, corresponding to a computational speedup of approximately three orders of magnitude. This substantial reduction in computation time makes the proposed framework particularly attractive for rapid design-space exploration and antenna optimization.

To further validate the predictive capability of the proposed model, Fig. 10 shows a predicted versus simulated scatter plot. Most data points lie close to the 45° reference line, indicating excellent agreement between predicted and simulated S_{11} values.

In this study, we distinguished two levels of validation. Model accuracy across the design space was obtained using the 100-sample held-out test set, which spanned the full trained parameter range rather than a single design point. In contrast, physical validation via fabrication and measurement is currently limited to the single reported prototype; extending physical validation to additional configurations spanning different regions of the design space is identified as future experimental work.

Fig. 11 illustrates the prediction error distribution. The error values were centered near zero and showed an approximately symmetric distribution, indicating that the regression model did not introduce systematic prediction bias. Furthermore, most prediction errors remained within ± 1 dB, confirming the robustness and reliability of the proposed surrogate model over the investigated design space.

Overall, the obtained results demonstrate that the proposed SVR-based surrogate model accurately predicts the reflection coefficient response of the AMC-PEC metasurface antenna

TABLE 6. Comparison with existing literature.

Ref.	Method	Samples	Predicted Output	Best R^2	Error	Fabricated & measured
Dai et al. [12], 2022	SVR (Gaussian kernel)	108	Resonant frequency (single value)	0.9736 (train)/ 0.9116 (test)	Not reported	Yes
Mersani et al. [27], 2025	KNN/MLP (best of 6 tested)	55,053	S_{11} (return loss)	> 0.98	Not reported	No (simulation-only)
Roy et al. [30], 2026	GBR/RFR/ XGBR/KNN	1,118	S_{11}, freq., gain, AR + inverse geometry	0.86–0.97 (best parameters)	Varies by parameter	Yes
Islam et al. [29], 2026	ANN/RF	100	S_{11}, BW, VSWR, gain, directivity	> 0.97	$< 1.5\%$ MAE	No (not yet validated)
This Work (Proposed)	**SVR (RBF)**	**500**	**Full S_{11} response curve**	**0.998**	**0.20 dB MAE/ 0.26 dB RMSE**	**Yes**

while reducing prediction time from several minutes of full-wave simulation to less than one second after model training. Consequently, the proposed framework provides an efficient surrogate modeling approach for rapid antenna design exploration, impedance optimization, and significantly reduced computational costs. Table 6 shows a comparison of the dataset size, prediction target, reported accuracy, and experimental validation status of the current study with four such representative studies.

As summarized in Table 6, the proposed SVR framework achieved the highest reported coefficient of determination ($R^2 = 0.998$) among the compared studies, while requiring substantially fewer training samples than the largest dataset in the group; achieving this accuracy with only 500 simulated samples, compared with the 55,053 samples required in [27], highlights the sample efficiency of the proposed surrogate modeling approach. Furthermore, the proposed model is one of only three studies in this comparison, alongside [12] and [30], to validate its predictions against a fabricated and measured prototype rather than simulation results alone, and it is the only one of the three to predict the full S_{11} response curve rather than a single scalar output such as resonant frequency [12]. These results collectively indicate that the proposed framework offers a favorable balance of prediction accuracy, dataset efficiency, and experimental validation relative to comparable machine-learning-assisted antenna modeling studies.

6. CONCLUSION

This study presents an SVR-based framework for rapidly predicting the S_{11} response of an X-band AMC-PEC metasurface antenna array. The regression model was trained using an openEMS-generated parametric dataset, with the antenna geometrical parameters as input features and the corresponding S_{11} response as the target variable. Once trained, the proposed model predicts the S_{11} response without requiring repeated full-wave electromagnetic simulations, substantially reducing the computational effort during antenna design and optimization.

The predicted responses showed excellent agreement with both full-wave simulations and experimental measurements, demonstrating that the proposed framework effectively captures the nonlinear relationship between the antenna geometry and its impedance characteristics. Prediction accuracy was quantified using standard statistical metrics, yielding an MAE of 0.20 dB, RMSE of 0.26 dB, and R^2 value of 0.998, demonstrating high-fidelity prediction of the S_{11} response over the operating band.

The present surrogate model was trained using four geometric parameters (AMC unit cell patch size, PEC patch size, ground-plane slot width, and substrate thickness), each of which varied within the ranges given in Section 3. Predictions are reliable in these trained ranges; extrapolation beyond them or to parameters not included in this study (e.g., substrate permittivity, unit cell periodicity, or array size) is not guaranteed and would require retraining on an expanded dataset. In addition, unlike the GPR benchmark evaluated in this study, the SVR formulation used here provides a point estimate without a native measure of prediction uncertainty, which is a practical limitation of design-support tools. Future work will address this using bootstrap-resampled SVR ensembles or quantile-regression SVR to construct prediction intervals. In the interim, the GPR model can be deployed alongside the SVR point estimate, in which confidence bounds are required. In future work, we will extend the design space to include additional geometric and material parameters and extend the surrogate to predict multiple electromagnetic outputs simultaneously (e.g., gain and radar cross-section reduction) from the same input parameterization, enabling a multi-objective (Pareto) design search rather than a single-objective (S_{11}) prediction. Recent work on AI-based multi-objective antenna tuning [26] demonstrates the viability of this approach using surrogate models of the type developed here.

The proposed methodology provides an efficient design-support tool for rapid impedance prediction, design space exploration, and optimization of AMC-PEC metasurface antennas while significantly reducing simulation time. Although this study employs kernel-based regression, recent advances in deep learning have demonstrated considerable potential for inverse electromagnetic design and high-dimensional optimization [23–25]. Ensemble regressors offer a comparable near-term route, as demonstrated by the experimental validation of forward and inverse metasurface-antenna modeling using Gradient Boosting, Random Forest, XGBoost, and KNN regressors on a dataset of 1,118 samples [30]. In future work, the proposed framework will be extended to deep learning-based surrogate models for larger datasets, broader operating bandwidths, and more complex geometries.

REFERENCES

[1] Iyer, A. K., A. Alu, and A. Epstein, "Metamaterials and metasurfaces-historical context, recent advances, and future directions," *IEEE Transactions on Antennas and Propagation*, Vol. 68, 1223–1231, March 2020.

[2] Holloway, C. L., E. F. Kuester, J. A. Gordon, J. O'Hara, J. Booth, and D. R. Smith, "An overview of the theory and applications of metasurfaces: The two-dimensional equivalents of metamaterials," *IEEE Antennas and Propagation Magazine*, Vol. 54, 10–35, April 2012.

[3] Yu, N., P. Genevet, M. A. Kats, F. Aieta, J.-P. Tetienne, F. Capasso, and Z. Gaburro, "Light propagation with phase discontinuities: Generalized laws of reflection and refraction," *Science*, Vol. 334, 333–337, October 2011.

[4] Cui, T. J., M. Q. Qi, X. Wan, J. Zhao, and Q. Cheng, "Coding metamaterials, digital metamaterials and programmable metamaterials," *Light: Science & Applications*, Vol. 3, e218, October 2014.

[5] Zou, H., S. Zeng, C. Li, and J. Ji, "A survey of machine learning and evolutionary computation for antenna modeling and optimization: Methods and challenges," *Engineering Applications of Artificial Intelligence*, Vol. 138, 109381, December 2024.

[6] Murugesan, A., K. T. Selvan, A. Iyer, K. V. Srivastava, and A. Alphones, "A review of metasurface-assisted RCS reduction techniques," *Progress In Electromagnetics Research B*, Vol. 94, 75–103, 2021.

[7] Prado, D. R., J. A. Lopez-Fernandez, G. Barquero, M. Arrebola, and F. Las-Heras, "Fast and accurate modeling of dual-polarized reflectarray unit cells using support vector machines," *IEEE Transactions on Antennas and Propagation*, Vol. 66, 1258–1270, March 2018.

[8] Reddy, K. J., R. V. Kumar, M. V. D. P. Kumar, and B. Mamatha, "AI-driven metamaterial antenna design: A review," *International Journal of Intelligent Systems and Applications in Engineering*, Vol. 12, No. 4, 5571, 2024.

[9] Akinsolu, M. O., K. K. Mistry, B. Liu, P. I. Lazaridis, and P. Excell, "Machine learning-assisted antenna design optimization: A review and the state-of-the-art," in *2020 14th European Conference on Antennas and Propagation (EuCAP)*, 1–5, Copenhagen, Denmark, March 2020.

[10] El Misilmani, H. M., T. Naous, and S. K. A. Khatib, "A review on the design and optimization of antennas using machine learning algorithms and techniques," *International Journal of RF and Microwave Computer-Aided Engineering*, Vol. 30, July 2020.

[11] Patel, S. K., J. Surve, V. Katkar, and J. Parmar, "Machine learning assisted metamaterial-based reconfigurable antenna for low-cost portable electronic devices," *Scientific Reports*, Vol. 12, Article number 12354, July 2022.

[12] Dai, X. W., D. L. Mi, H. T. Wu, and Y. H. Zhang, "Design of compact patch antenna based on support vector regression," *Radioengineering*, Vol. 31, 339–345, September 2022.

[13] Pedregosa, F., G. Varoquaux, A. Gramfort, V. Michel, B. Thirion, O. Grisel, M. Blondel, P. Prettenhofer, R. Weiss, V. Dubourg, J. Vanderplas, A. Passos, D. Cournapeau, M. Brucher, M. Perrot, and E. Duchesnay, "Scikit-learn: Machine learning in python," *Journal of Machine Learning Research*, Vol. 12, No. 85, 2825–2830, 2011.

[14] Liebig, T., A. Rennings, S. Held, and D. Erni, "OpenEMS — A free and open source equivalent-circuit (EC) FDTD simulation platform supporting cylindrical coordinates suitable for the analysis of traveling wave MRI applications," *International Journal of Numerical Modelling: Electronic Networks, Devices and Fields*, Vol. 26, 680–696, December 2012.

[15] Angiulli, G., M. Cacciola, and M. Versaci, "Microwave devices and antennas modelling by support vector regression machines," *IEEE Transactions on Magnetics*, Vol. 43, 1589–1592, April 2007.

[16] Jacobs, J. P., "Efficient resonant frequency modeling for dual-band microstrip antennas by gaussian process regression," *IEEE Antennas and Wireless Propagation Letters*, Vol. 14, 337–341, 2015.

[17] Wu, Y., Z. Tang, Y. Xu, Y. Guo, and B. Zhang, "Support vector regression for measuring electromagnetic parameters of magnetic thin-film materials," *IEEE Transactions on Magnetics*, Vol. 43, 4071–4075, December 2007.

[18] Vapnik, V. N., *Statistical Learning Theory*, Wiley, 1998.

[19] Smola, A. J. and B. Schölkopf, "A tutorial on support vector regression," *Statistics and Computing*, Vol. 14, 199–222, August 2004.

[20] Koziel, S. and X.-S. Yang, *Computational Optimization, Methods and Algorithms*, Springer Science & Business Media, 2011.

[21] Jin, J.-M., *Theory and Computation of Electromagnetic Fields*, Wiley, 2015.

[22] Williams, C. K. I. and C. E. Rasmussen, *Gaussian Processes for Machine Learning*, MIT Press, 2006.

[23] Ma, W., Z. Liu, Z. A. Kudyshev, A. Boltasseva, W. Cai, and Y. Liu, "Deep learning for the design of photonic structures," *Nature Photonics*, Vol. 15, 77–90, October 2020.

[24] Liu, D., Y. Tan, E. Khoram, and Z. Yu, "Training deep neural networks for the inverse design of nanophotonic structures," *ACS Photonics*, Vol. 5, 1365–1369, February 2018.

[25] So, S., T. Badloe, J. Noh, J. Rho, and J. Bravo-Abad, "Deep learning enabled inverse design in nanophotonics," *Nanophotonics*, Vol. 9, 1041–1057, February 2020.

[26] Koziel, S., A. Pietrenko-Dabrowska, and S. Szczepanski, "Multi-objective artificial-intelligence-based parameter tuning of antennas using variable-fidelity machine learning," *Scientific Reports*, Vol. 15, Article number 21693, July 2025.

[27] Mersani, and A., K. Mekki, and O. Ncibi, "AI-powered S_{11} prediction for a compact 2.4 GHz patch antenna," *Indian Journal Of Science And Technology*, Vol. 18, 2715–2728, September 2025.

[28] Boulaich, M. H., S. Ohamouddou, M. A. Ennasar, and A. E. Afia, "AI-assisted metasurface antennas design/optimization and performance enhancement techniques: A comprehensive survey," *IEEE Access*, Vol. 14, 29 803–29 835, 2026.

[29] Islam, M. B., A. N. M. S. Uddin, S. Bashir, P. K. Paul, M. F. Ahmed, and M. H. Kabir, "Design optimization of a C/X-band metasurface–DGS microstrip antenna using machine learning," *Physics Open*, Vol. 27, 100419, May 2026.

[30] Roy, H., T. Khan, and M. Maqbul, "Machine learning-based forward and inverse modeling framework for metasurface-aided antennas in 5G sub-6 GHz wireless power harvesting environments," *AEU — International Journal of Electronics and Communications*, Vol. 213, 156361, July 2026.